

Enhanced visible and near-infrared capabilities of the JET mirror-linked divertor spectroscopy system)

B. A. Lomanowski, A. G. Meigs, N. J. Conway, K.-D. Zastrow, R. M. Sharples, P. Heesterman, D. Kinna, and JET EFDA Contributors

Citation: *Review of Scientific Instruments* **85**, 11E432 (2014); doi: 10.1063/1.4893426

View online: <http://dx.doi.org/10.1063/1.4893426>

View Table of Contents: <http://scitation.aip.org/content/aip/journal/rsi/85/11?ver=pdfcov>

Published by the [AIP Publishing](#)

Articles you may be interested in

[Near-infrared spectroscopy for divertor plasma diagnosis and control in DIII-D tokamak](#)

Rev. Sci. Instrum. **85**, 11E418 (2014); 10.1063/1.4891600

[Coherence imaging of scrape-off-layer and divertor impurity flows in the Mega Amp Spherical Tokamak \(invited\)a\)](#)

Rev. Sci. Instrum. **85**, 11D703 (2014); 10.1063/1.4891165

[Development of a mirror-based endoscope for divertor spectroscopy on JET with the new ITER-like wall \(invited\)a\)](#)

Rev. Sci. Instrum. **83**, 10D511 (2012); 10.1063/1.4731759

[Enhancement of JET's mirror-link near-ultraviolet to near-infrared divertor spectroscopy system\)](#)

Rev. Sci. Instrum. **81**, 10E532 (2010); 10.1063/1.3502322

[Enhanced core charge exchange recombination spectroscopy system on Joint European Torus](#)

Rev. Sci. Instrum. **77**, 10F102 (2006); 10.1063/1.2222170



You don't still use this cell phone

or this computer

Why are you still using an AFM designed in the 80's?

It is time to upgrade your AFM

Minimum \$20,000 trade-in discount for purchases before August 31st

Asylum Research is today's technology leader in AFM

dropmyoldAFM@oxinst.com

OXFORD
INSTRUMENTS

The Business of Science®

Enhanced visible and near-infrared capabilities of the JET mirror-linked divertor spectroscopy system^{a)}

B. A. Lomanowski,^{1,b)} A. G. Meigs,² N. J. Conway,² K.-D. Zastrow,² R. M. Sharples,¹ P. Heesterman,² D. Kinna,² and JET EFDA Contributors^{c)}

JET-EFDA, Culham Science Centre, Abingdon OX14 3DB, United Kingdom

¹*Centre for Advanced Instrumentation, Department of Physics, Durham University, Durham DH1 3LE, United Kingdom*

²*EURATOM/CCFE Fusion Association, Culham Science Center, Abingdon OX14 3DB, United Kingdom*

(Presented 4 June 2014; received 4 June 2014; accepted 30 July 2014; published online 18 September 2014)

The mirror-linked divertor spectroscopy diagnostic on JET has been upgraded with a new visible and near-infrared grating and filtered spectroscopy system. New capabilities include extended near-infrared coverage up to 1875 nm, capturing the hydrogen Paschen series, as well as a 2 kHz frame rate filtered imaging camera system for fast measurements of impurity (Be II) and deuterium D α , D β , D γ line emission in the outer divertor. The expanded system provides unique capabilities for studying spatially resolved divertor plasma dynamics at near-ELM resolved timescales as well as a test bed for feasibility assessment of near-infrared spectroscopy. [<http://dx.doi.org/10.1063/1.4893426>]

I. INTRODUCTION

The mirror-linked divertor spectroscopy system¹ on JET provides spatially resolved passive spectroscopy measurements of plasma emission from the outer divertor. The system covers a total spectral range of 350–1000 nm. In preparation for the JET ITER-like wall (ILW) campaigns the system was upgraded in 2008 with an extended field of view (FOV) (150 mm to 360 mm) and increased optical throughput.²

Following the 2013 JET-ILW campaign further opportunities were identified for improving the system, namely:

- Extending the near-infrared spectral coverage to 1875 nm
- Increasing the time resolution of Balmer series and Be line intensity spatially resolved measurements up to $\sim 500 \mu\text{s}$
- Increasing the wavelength window for dedicated Balmer series measurements

Spectroscopy in the near-infrared range offers the potential of increased tolerance to the degradation of optics under a harsh burning plasma environment,³ but plasma emission in the 1000–1875 nm range is poorly characterized at present.

Improved time resolution and a dedicated Balmer series monitor offer enhanced capabilities for divertor characterization and physics studies of plasma detachment. The high density, low temperature recombining region characteristic of the detached plasma regime results in a reduction of steady-state heat and particle fluxes to the divertor tiles. In ELMy H-mode plasmas this mechanism is periodically interrupted

by edge localized modes (ELMs) which deposit a significant portion of the stored plasma energy onto the divertor tiles on timescales of $\sim 100 \mu\text{s}$. The plasma dynamics and the interplay between ELM power deposition and plasma detachment are not well understood.

II. DIAGNOSTIC OVERVIEW

The new visible system consists of an additional imaging spectrometer (KT3E) and two imaging filter-scope cameras (KT3-E8TA/B) for spatially resolved Balmer series and impurity line emission measurements in the 390–700 nm range. A notable feature of the grating spectrograph is the Schmidt-Czerny-Turner design which improves imaging quality over a traditional Czerny-Turner by greatly reducing astigmatism and coma across the focal plane while providing an $f/4.6$ input beam for increased throughput.

The near-infrared system extends the diagnostic spectral range to 1875 nm. A single chord, low resolution compact spectrometer, utilizing a volume phase grating, provides surveying capability from 900–1700 nm, and a filter-scope photodiode system provides access to the deuterium Paschen alpha line at 1874.6 nm. Table I summarizes the specifications of the new visible and near-infrared systems.

III. DESIGN

The mirror-linked optical train can be conceptually visualized by unfolding the optical path and removing the flat relay mirrors. Fig. 1(a) shows the remaining optical components: an objective lens (lens A), a field mirror (mirror D), and focusing optics in the roof lab. The FOV with $h_o = 360$ mm is limited by the vessel port geometry (Fig. 1(b)) whereas the biological penetration limits the light collection area upstream. In the roof lab, a pseudo-collimated on-axis beam of diameter $\varphi_r = 130$ mm intercepts the primary mirrors of Newtonian telescopes which focus the intermediate divertor image onto the entrance slits of spectrometers KT3A, KT3B,

^{a)}Contributed paper, published as part of the Proceedings of the 20th Topical Conference on High-Temperature Plasma Diagnostics, Atlanta, Georgia, USA, June 2014.

^{b)}Author to whom correspondence should be addressed. Electronic mail: b.a.lomanowski@durham.ac.uk

^{c)}See the Appendix of F. Romanelli *et al.*, Proceedings of the 24th IAEA Fusion Energy Conference 2012, San Diego, USA.

TABLE I. System specifications.

	Desc.	Specifications
KT3D	NIR spec., filtered $P\alpha$ photo-diodes	Model (spec.): BaySpec NIRS-900-1700 Range (spec.): 900–1700 nm λ res. (spec.): 7 nm FWHM Aperture ratio: $f/2.0$ Time res.: 50–250 ms Spatial res.: single chord, full FOV Model (ph.diodes): Hamamatsu G12182-210K $P\alpha$ filter: 4.5 nm FWHM
KT3E	0.32 m Schmidt Czerny-Turner imaging spec.	Model: Princeton Inst. IsoPlane SCT-320 Range: 390–700 nm Gratings: 200, 1200, 1800 l/mm Focal length, aperture: 0.32 m, $f/4.6$ Time res.: 15–40 ms Spatial res. (binned): 15 mm
KT3 E8TA/ E8TB	Filtered imaging spec.	Model: AVT Pike F-032 Filters: $D\alpha$, $D\beta$, $D\gamma$, Be II 436.0/ 467.3 nm @ 1.5 nm FWHM Time res.: $\geq 500 \mu\text{s}$ Spatial res. (no binning): 1.2 mm/pixel

and KT3C. Off-axis points are vignetted as a function of the field angle θ_o by the penetration tube down to $\varphi_r \approx 90$ mm.

The basis of the new optical system is the utilization of the beam area that is obstructed by the Newtonian secondary mirrors (Fig. 1(c)).

The turning mirror of diameter $\varphi_r' = 27$ mm placed behind the Newtonian secondary mirror cell becomes the aperture stop, reducing the throughput by a factor of 10 on axis and up to 22 for the maximum field angle.

Selection of CCDs for the visible system was largely based on the application requirements for sensitivity and speed. For the new grating spectrometer (KT3E) a 1024×1024 pixel frame transfer cooled CCD (ProEM 1024B) offers excellent quantum efficiency (QE) with a peak of $\sim 95\%$ at 650 nm and very low dark current of $0.002 e^-/\text{pixel/s}$ at -50°C .

Two interline CCD cameras (AVT Pike F-032) provide frame rates up to ~ 2 kHz for the visible filtered imaging system (KT3-E8TA/B). Although the QE suffers due to lower fill

factors, microlenses recover much of the QE with a peak of $\sim 54\%$ at 500 nm for the KAI-0340 640×480 sensors. With fast charge transfer, short exposure times and minimized image smear, interline CCDs offer a good compromise between sensitivity and speed.

Detection in the near-infrared system (KT3D) is based on the Indium Gallium Arsenide (InGaAs) photodiode technology. Band gap energies of InGaAs detectors can be tuned by changing the composition ratio of In and Ga. The standard type offers good spectral response in the 900–1700 nm range while extended-InGaAs photodiodes provide cut-offs up to 2600 nm.

The near-infrared spectroscopy detectors consist of a cooled (-5°C) standard-InGaAs 256 pixel linear array used in the grating spectrometer, and two extended-InGaAs 1 mm diameter cooled (-20°C) photodiodes for the Paschen alpha filter-scope. The two photodiodes are operated in photovoltaic mode in which the thermal or Johnson noise dominates over dark current noise.⁴

The visible and near-infrared filter-scopes employ 2-cavity Fabry-Perot interference filters with a narrowband transmission profile of $\sim 3.5 \times \text{FWHM}$ at 1% peak transmission. Filters in the visible system limit the bandpass to 1.5 nm FWHM while the Paschen alpha line ($P\alpha$, 1874.6 nm) and $P\alpha$ background correction (1886 nm) filters provide a 4.5 nm FWHM bandpass. A narrower bandpass in the near-infrared can technically be achieved but at substantial additional cost relative to the visible range filters. The small ($<0.5^\circ$) incidence and field angles of the pseudo-collimated light incident on the bandpass filters result in a negligible center wavelength shift (<0.03 nm) for all rays across the pupil.

IV. DIAGNOSTIC PERFORMANCE

A. Visible system

The available light at the secondary turning mirrors of the new visible and near-infrared systems is estimated from

$$P_\lambda = L_\lambda GT_\lambda, \quad (1)$$

where P_λ is the total photon flux [$\text{ph s}^{-1} \text{nm}^{-1}$] incident on the secondary turning mirror, L_λ is the averaged spectral radiance

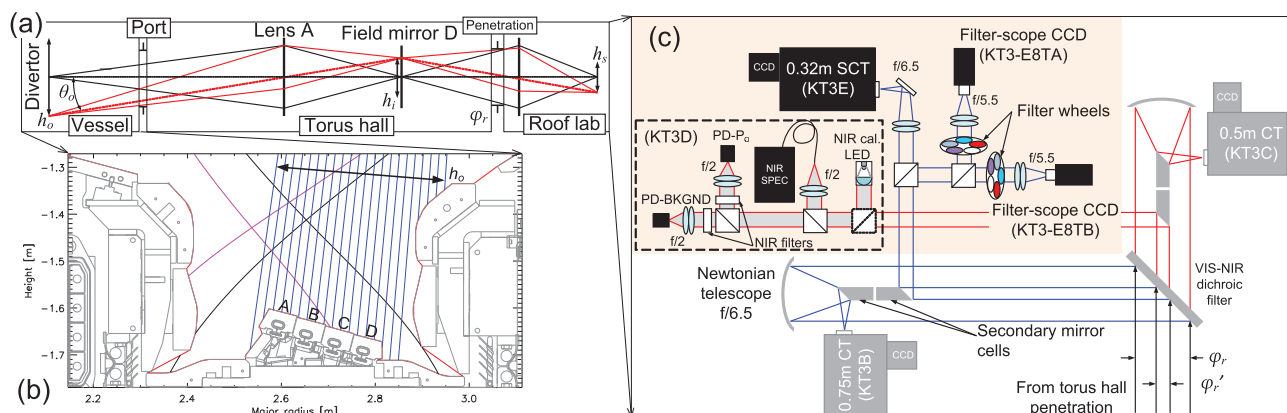


FIG. 1. (a) Optical layout of the mirror-linked divertor spectroscopy system; (b) viewing geometry (blue) of the JET-ILW divertor with horizontal (magenta) and vertical (black) plasma configuration and solid horizontal tungsten tile segments A, B, C, and D; (c) roof lab layout of the existing (grey) and new (black) systems.

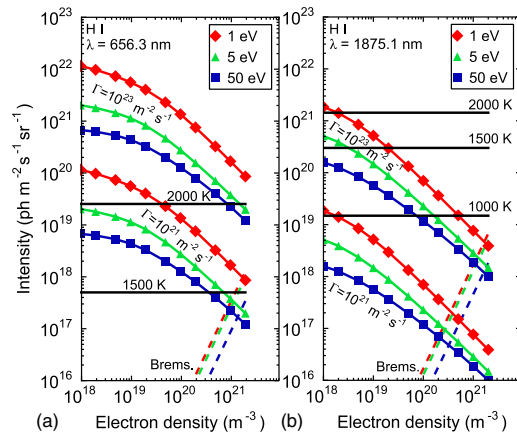


FIG. 2. Line intensity estimates: (a) H α , 1.5 nm FWHM bandpass; (b) P α , 4.5 nm FWHM bandpass.

[$\text{ph s}^{-1} \text{m}^{-2} \text{sr}^{-1} \text{nm}^{-1}$] across the divertor FOV, G is the averaged etendue [$\text{m}^2 \text{sr}$] across the field, and T_λ is the total spectral optical transmission. Estimated values are $G = 1.07 \times 10^{-8} [\text{m}^2 \text{sr}]$ and $T_\lambda = 0.15$ in the range 300–2000 nm.

Based on observations of the outer divertor deuterium ion fluxes in JET-ILW discharges^{5,6} and using inverse photon efficiency (S/XB) coefficients from ADAS⁷ with an influx in the range $10^{21} \leq \Gamma \leq 10^{23} [\text{m}^{-2} \text{s}^{-1}]$, the expected D α radiance averaged across the outer divertor is shown in Fig. 2(a) assuming a line of sight integration of emissivity ε through 100 mm of an isothermal divertor plasma. With a 50 μm slit width, 3 mm image height, and 200 l/mm grating, the estimated signal-to-noise (SNR) for D α spectroscopy on KT3E is $150 \leq \text{SNR} \leq 5500$ assuming a total CCD noise of 6 e^- RMS and 25 fps frame rate. Similarly, the SNR for the Pike cameras with a D α filter and a 2.4 mm image height yields values of $10 \leq \text{SNR} \leq 350$ assuming 1 kHz fps and 16 e^- RMS camera noise. On-chip and post-process binning will improve the SNR by a factor 3–5 for lower intensity lines.

Fig. 2(a) also shows the estimated Bremsstrahlung (using the approach in Ref. 8), and thermal contributions from the outer divertor plasma and tungsten tiles. Free-bound emission is ignored. Thermal emission includes a temperature dependent tungsten emissivity estimate.⁹ The broadband emission was then multiplied by a 1.5 nm FWHM bandpass centered on the D α wavelength.

B. Near-infrared system

The estimated range of hydrogen Paschen alpha (P α , $n = 4-3$) radiance is shown in Fig. 2(b). The D α /P α ratio is in the range 10–20 for ionizing plasma conditions in the range $1 \leq T_e \leq 50 \text{ eV}$ and $10^{19} \leq n_e \leq 10^{21} \text{ m}^{-3}$. The Paschen beta line (P β , $n = 5-3$, 1281.8 nm) is weaker than P α by a factor of 6–7 in the same range.

The NIR spectrometer and P α filter-scope collect light from the entire divertor FOV. With a 50 μm slit width, 50 $\mu\text{m} \times 500 \mu\text{m}$ pixels, and a line width of 2.2 pixels FWHM, the estimated SNR for P β grating spectroscopy is $30 \leq \text{SNR} \leq 300$ at 100 ms exposure.

The P α photocurrent is estimated to be in the range $0.2 \leq i \leq 20 \mu\text{A}$, for which the SNR is $30 \leq \text{SNR} \leq 300$ given

a detectivity $D^* = 2 \times 10^{12} [\text{cmHz}^{1/2}/\text{W}]$ at a measurement bandwidth of 20 Hz. An avalanche photodiode (APD) could provide additional gain to improve the measurement bandwidth, but, although readily available in the standard-InGaAs range, an extended-InGaAs APD is currently a custom product and incurs significant additional cost.

Near-infrared measurements are complicated by a larger contribution of surface thermal emission. Fig. 2(b) includes estimates of the thermal emission for representative tungsten tile temperatures with a bandpass of 4.5 nm FWHM. The Bremsstrahlung contribution is also shown. Similar to the visible range, signal contamination from Bremsstrahlung only becomes significant for high electron density and low electron temperatures.

Removing the background contribution from the P α signal is achieved by a separate 4.5 nm FWHM bandpass filter offset from the P α deuterium line by 11 nm, limiting crosstalk between the two measurements to $\sim 1\%$. Contamination from impurity line emission is expected to have negligible contribution. The Planckian radiation from tungsten tiles adds a non-linear component to the corrected P α signal, resulting in an uncertainty which increases with temperature up to $\pm 5\%$ in the range $1000 \text{ K} \leq T \leq 2000 \text{ K}$.

V. INITIAL RESULTS

Preliminary results from the NIR spectrometer are shown in Fig. 3 with the strong lines from intrinsic impurities (Be I, Be II, C I) and the P β and P γ lines identified. Thermal emission from the stack of tungsten divertor tiles contributes a significant broadband component in the spectrum of pulse 85829. A region of poor transmission around 1380 nm is also evident in the raw data. The presence of the thermal spectrum reduces the dynamic range for line emission intensity measurements, but provides spectrally resolved temperature data useful for IR thermography. Quantitative measurements of spectral line emission intensities and line profiles are possible given a suitable background subtraction technique, provided the sum of emission components does not saturate the detector.

Initial results of the filtered imaging camera measurements with a D α filter and 1 kHz frame rate are shown in Fig. 4 for two JET pulses exhibiting H-mode. In JET-ILW the occurrence of ELMs is indicated by the Be II line emission (527 nm) as shown in Figs. 4(a) and 4(b) for the inner and outer divertor photo-multiplier (PMT) channels. The collapse

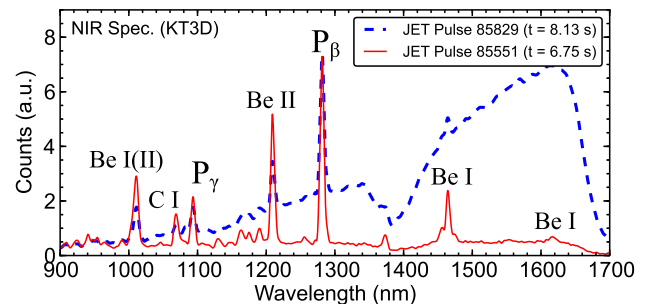


FIG. 3. NIR spectra in 2.0 MA, 13 MW NBI, and 3.3 MW ICHR heated plasma (85829) and 2.0 MA ohmically heated plasma during a density limit disruption (85551).

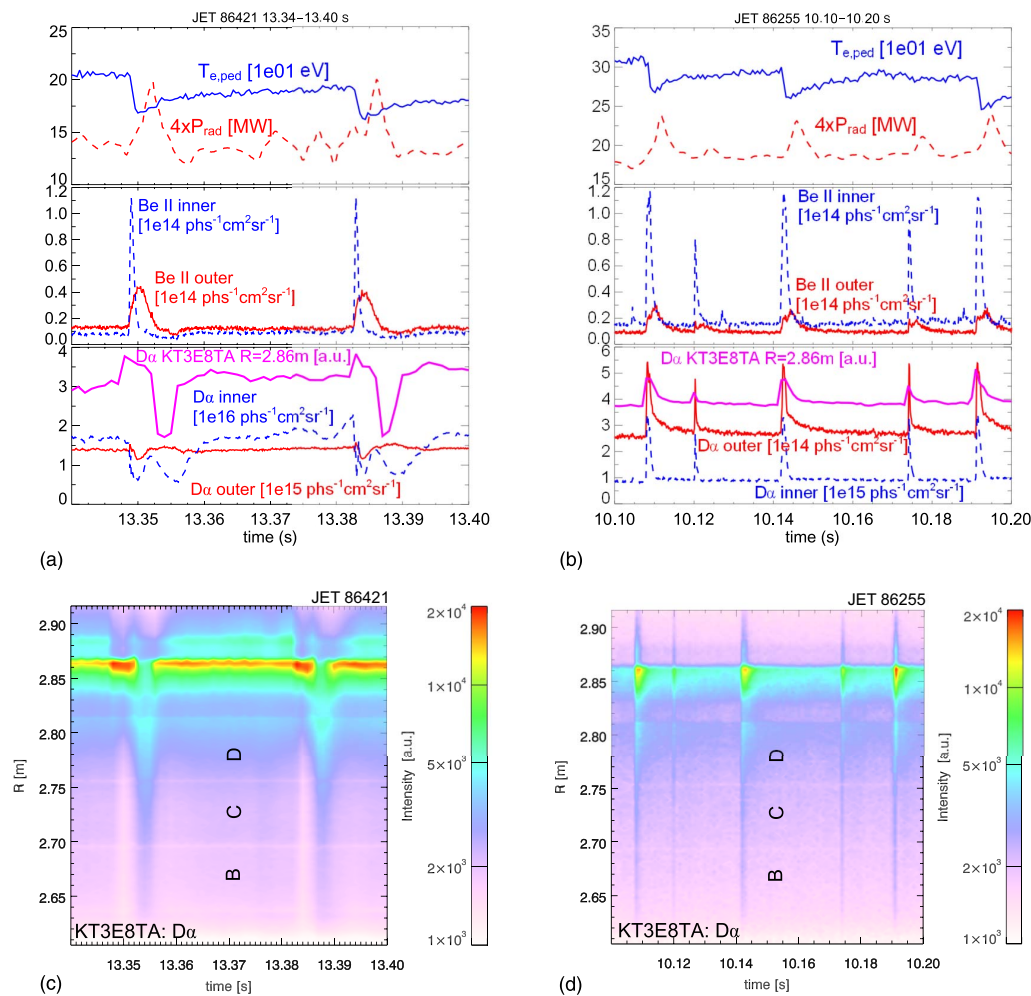


FIG. 4. (a) ELM cycles in JET pulse 86421, 1.8 MA, 2.3 T, 6 MW NBI; (b) ELM cycles in JET pulse 86255, 2.0 MA, 2.9 T, 7 MW NBI; (c, d) $D\alpha$ outer divertor radial profiles from filtered imaging camera KT3E8TA with indicated locations of the horizontal tungsten tile stacks B, C, and D (see Fig. 1(b) for poloidal cross section of the JET-ILW divertor).

in pedestal temperature and subsequent peak in radiated power are also consistent with ELM cycles. $D\alpha$ divertor line emission is not a reliable ELM indicator when a cold and dense plasma region forms near the strike points. The upper states of the deuterium series transitions can then be populated mainly by recombination rather than excitation, leading to a sudden dip in the $D\alpha$ signal as the cold and dense region collapses during the ELM in contrast to the more common $D\alpha$ spike associated with increased wall recycling. The inner and outer $D\alpha$ PMT channels for pulse 86421 show such an inversion, whereas the more conventional $D\alpha$ spike is observed in pulse 86255.

Figs. 4(c) and 4(d) demonstrate the first of its kind $D\alpha$ measurements at ELM-resolved timescales and 1.2 mm spatial resolution along the outer divertor for the pulses shown in Figs. 4(a) and 4(b). A spatial chord from the filtered camera data at $R = 2.86$ m is also shown in Figs. 4(a) and 4(b). The radial profiles exhibit the two types of $D\alpha$ ELM signatures (dips vs. spikes) discussed and demonstrate the diagnostic potential for improved divertor characterization and physics studies associated with transient atomic processes in detached plasmas (e.g., profiles of the $D\gamma/D\alpha$ ratio using the pair of filtered imaging cameras).

ACKNOWLEDGMENTS

This work, supported by the European Communities under the contract of Association between EURATOM and CCFE, was carried out within the framework of the European Fusion Development Agreement. The views and opinions expressed herein do not necessarily reflect those of the European Commission. The work was also partly funded by the United Kingdom Engineering and Physical Research Council under Grant No. EP/K504178/1.

¹A. Meigs *et al.*, *Rev. Sci. Instrum.* **81**, 10E532 (2010).

²A. Meigs *et al.*, in Proceedings of the 20th International Conference on Plasma Surface Interactions, Aachen, Germany, 2012.

³V. A. Soukhanovskii, *Rev. Sci. Instrum.* **79**, 10F539 (2008).

⁴A. Rogalski, *Infrared Detectors*, 2nd ed. (Taylor & Francis, Boca Raton, 2011).

⁵F. Romanelli and JET EFDA Contributors, *Nucl. Fusion* **53**, 104002 (2013).

⁶A. Huber *et al.*, *J. Nucl. Mater.* **438**, S139–S147 (2013).

⁷H. P. Summers, The ADAS User Manual, version 2.6, see <http://adas.phys.strath.ac.uk>, 2004.

⁸A. T. Ramsey and S. L. Turner, *Rev. Sci. Instrum.* **58**, 1211 (1987).

⁹J. W. Davis and P. D. Smith, *J. Nucl. Mater.* **233–237**(2), 1593–1596 (1996).